Time-resolved Compton scattering for a model fermion-boson system

R. E. Wagner, Q. Su, and R. Grobe

Intense Laser Physics Theory Unit and Department of Physics, Illinois State University, Normal, Illinois 61790-4560, USA
(Received 1 June 2010; published 30 August 2010)

We study the scattering of a boson with a fermion with full spatial and temporal resolution based on the one-dimensional Yukawa Hamiltonian. In quantum field theory this interaction is described by the annihilation and creation of bosons with intermediate virtual particle states. We show that this process can be modeled in the center-of-mass frame by a scattering potential, permitting us to interpret the absorption and re-emission processes in quantum mechanical terms of a characteristic force. This Compton force between the fermion and boson is repulsive for large distances and attractive for shorter spacings. We also examine the periodic dynamics of a fermion and a boson that are spatially confined to a ring cavity in which they counterpropagate, enabling us to study interactions independent of the transients that characterize the (one-time) scattering event of two wave packets.

PACS number(s): 03.65.Nk

I. INTRODUCTION

In a ground-breaking work in 1923, Compton studied the scattering of x rays off electrons bound in light elements [1]. Using quantum theory for the photons, he provided an explanation for the observed increase of the wavelength due to the scattering and its quantitative relationship with the Compton wavelength of the electron and the scattering angle. In contrast to the predictions of earlier work by Thompson on elastic scattering, Compton showed that the energy loss of the scattered beam is identical to the gain in recoil kinetic energy of the electron. He also confirmed the calculated intensity distribution for the scattered radiation in experiments in graphite. This seminal work was one of the first illustrations that a radiation quantum carries energy as well as momentum, illustrating the wave-particle dualism of electromagnetic fields long before quantum field theory [2–4] was developed.

While many experimental predictions for colliding monoenergetic electron beams have been confirmed with astonishing accuracy [5], to the best of our knowledge a detailed quantum field theoretical analysis that visualizes the interaction of fermions and bosons with full space-time resolution is presently lacking. In this work we use a simplified model system to examine the spatial dynamics of the photon absorption and re-emission processes for the collision of an incoming boson wave packet with a spatially localized fermion. The initial goal is not to make quantitative predictions for a specific experimental realization, but to introduce a theoretical framework to better understand the role virtual and dressing bosons play when a physical fermion interacts with its environment [6,7]. For example, in the case of the Coulombic interaction between two fermions of equal or opposite charge, the dressing bosons are believed to be essential mediators for the force. The dynamical aspects of how the exchange of intermediary bosons can lead to attractive or repulsive forces between two fermions is presently not well understood [8].

In order to gain some insight into the quantum field theoretical dynamics and to get some experience with the computational and conceptual challenges, we have begun to analyze a system that was used in the 1950s by Yukawa to phenomenologically model the strong nuclear force and the interaction of nucleons with π mesons. Its Hamiltonian is almost identical to the Hamiltonian of quantum electrodynamics (QED), except that the electrons and positrons are coupled to a scalar (spinless) boson instead of the photon. In order to make the system computationally feasible, we reduce the spatial dimension to only one and permit the model photon to have a finite mass leading to only attractive interfermionic forces. It has no ultraviolet or infrared divergences, which makes it an ideal system for us to develop the quantum field theoretical framework to visualize interacting fermion-boson systems with full space and time resolution. In several recent works, we have used this system to test the predictions of the Greenberg-Schweber (recoil-free) approximation [2,9–11], to simulate the evolution of a bare particle into a physical particle by the generation of a cloud of bosons that surrounds the fermion [12], to examine the mutual coherence properties of bosons that were created by two spatially distinct regions of a single bare fermion state [13], and to study the impact of the photon dressing on the electron's physical mass [14].

The paper is structured as follows. In the second section, we introduce the quantum field theoretical system. In the third section, we discuss how a boson can be absorbed by a fermion during a scattering event. Using second-order perturbation theory, we find analytical approximations for the reflection coefficient and introduce the concept of a Compton force and discuss its properties. In the fourth section, we analyze the time evolution of the two particles in a ring cavity and examine the time scales associated with the virtual particles. In the fifth section, we study how the fermion and boson wave packets collide and focus on the time evolution of the virtual particles that are involved. We finish in the sixth section with a brief discussion and outlook on future work.

II. THE MODEL SYSTEM

We denote the quantum field operators for the spinless fermions (modeling electrons and positrons) and neutral scalar bosons (modeling photons) with $\hat{\Psi}(z)$ and $\hat{\varphi}(z)$, where z denotes the (one-dimensional) spatial coordinate. We can

expand these operators in momentum states,

$$\hat{\Psi}(z) \equiv \int dp \hat{b}(p)(2\pi)^{-1/2} u(p) \exp(ipz/\hbar)$$

$$+ \int dp \hat{d}(p)^{\dagger}(2\pi)^{-1/2} v(p) \exp(-ipz/\hbar), \quad (2.1a)$$

$$\hat{\varphi}(z) \equiv \int dk c\hbar^{1/2}[2\omega(k)]^{-1/2} \hat{a}(k)(2\pi)^{-1/2} \exp(ikz/\hbar) + \text{H.c.}, \quad (2.1b)$$

where the fermionic and bosonic creation and annihilation operators fulfill the anticommutator and commutator relationships, $[\hat{d}(p), \hat{d}(p')^{\dagger}]_{+} = [\hat{b}(p), \hat{b}(p')^{\dagger}]_{+} = \delta(p - p')$ and $[\hat{a}(k), \hat{a}(k')^{\dagger}]_{-} = \delta(k - k')$. The two-component spinor coefficients are defined as $u(p) \equiv \{1 + \{pc/[Mc^2 + E(p)]\}^2\}^{-1/2}\{1, pc/[Mc^2 + E(p)]\}^T$ and $v(p) \equiv \{1 + \{pc/[Mc^2 + E(p)]\}^2\}^{-1/2}\{-pc/[Mc^2 + E(p)], 1\}^T$, where we used Dirac matrices represented here in terms of the Pauli matrices, $\gamma^0 = \sigma_3$ and $\gamma^1 = \sigma_1$. We denote the free energies by $E(p) \equiv \sqrt{[M^2c^4 + c^2p^2]}$ and $\hbar\omega(k) \equiv [m^2c^4 + c^2k^2]^{1/2}$, where the bare masses of the fermion and boson are M and m, respectively. As a result we have the outer product $u(p)u^{\dagger}(p) + v(p)v^{\dagger}(p)$ equal to the 2×2 unit matrix and the individual spinor component fields associated with the canonical position and momentum satisfy the required relationships $[\hat{\Psi}_a(z_1), i\hat{\Psi}_b(z_2)^{\dagger}]_{+} = i\hbar\delta(z_1 - z_2)\delta_{a,b}$ for $a,b = 1,2$ and for the real bosons $[\hat{\varphi}(z_1), \hat{\Pi}(z_2)]_{-} = i\hbar\delta(z_1 - z_2)$, where we have defined the canonical momentum operator $\hat{\Pi}(z) = c^{-2}\partial_t\hat{\varphi}(z)$. The Hamiltonian density for our system is given by $H_{\text{Dirac}}(z) + H_{\text{KG}}(z) + H_{\text{int}}(z)$, where

$$H_{\text{Dirac}}(z) = -ic\hat{\Psi}(z)^{\dagger}\sigma_1\partial_z\hat{\Psi}(z) + Mc^2\hbar^{-1}\hat{\Psi}(z)^{\dagger}\sigma_3\hat{\Psi}(z), \quad (2.2a)$$

$$H_{\text{KG}}(z) = c^2\hat{\Pi}(z)^2 + [\partial_z\hat{\varphi}(z)]^2 + (mc/\hbar)^2\hat{\varphi}(z)^2, \quad (2.2b)$$

$$H_{\text{int}}(z) = \gamma c^{3/2}\hbar^{-3/2}\hat{\bar{\Psi}}(z)\hat{\Psi}(z)\hat{\varphi}(z), \quad (2.2c)$$

and the conjugate spinor $\hat{\bar{\Psi}}(x)$ is defined as $\hat{\Psi}^{\dagger}(x)\gamma^0$, where the dagger is the usual Hermitian conjugate. The interaction between the fermions and bosons is given by the interaction part of the Hamiltonian density $H_{\text{int}}(z)$ where we have included the factor $c^{3/2}$ such that the coupling constant γ has the units of mass. As is customary in atomic physics and quantum optics [15–18], we will use from now on atomic units where the speed of light $c = 137$ a.u., the electron's mass and charge $m = e = 1$ a.u. and $\hbar = 1$ a.u. In order to focus on the dynamics of the fermion with the bosons, we omit the coupling to the antifermions. The Hamiltonian can be obtained from the density by $H = \int dz\, H(z)$, leading to

$$H = \int dp E(p)\hat{b}(p)^{\dagger}\hat{b}(p) + \int dk\omega(k)\hat{a}(k)^{\dagger}\hat{a}(k) + V, \quad (2.3a)$$

$$V = \gamma c^{5/2} \int dp \int dk \Gamma(p,k)\hat{b}(p+k)^{\dagger}\hat{b}(p)[\hat{a}(k) + \hat{a}(-k)^{\dagger}]. \quad (2.3b)$$

The coupling function $\Gamma(p,k)$ is the result of the scalar product among the Dirac spinors and acts as a natural cutoff function as it decreases with increasing momenta p and k. It is

given [14] by $\Gamma(p,k) \equiv (E_{p+k}E_p + M^2c^4 - p(p+k)c^2)^{1/2}(8\pi\omega_k E_{p+k}E_p)^{-1/2}$.

In order to examine the dynamics, we have to compute the time evolution of the quantum field theoretical state $\|\Phi(t)\rangle\rangle$ as a solution to the equation of motion, $i\partial\|\Phi(t)\rangle\rangle/\partial t = H\|\Phi(t)\rangle\rangle$ for a given initial state $\|\Phi(0)\rangle\rangle$. The time-evolved state will be used to calculate the spatial probability density of the (bare) fermions via $\rho_f(z,t) \equiv \langle\langle\Phi(t)\|\hat{\Psi}(z)^{\dagger}\hat{\Psi}(z)\|\Phi(t)\rangle\rangle$ and similarly for the bosons.

III. PERTURBATIVE ANALYSIS OF COMPTON SCATTERING

A. The coupling associated with the s- and t-channels

Our initial state is characterized by a bare fermion of sharp momentum p and a bare boson of sharp momentum k (denoted by $\|p; k\rangle\rangle$), and it is associated with the total bare energy $E \equiv E(p) + \omega(k)$. The lowest-order energy and momentum conserving final state has the momenta p_f and k_f, with $p + k = p_f + k_f$ and $E = E(p_f) + \omega(k_f)$. In first order of the coupling constant γ, the Hamiltonian can either increase or decrease the number of bosons by 1 as shown in the diagrams of Fig. 1.

The downward transition (boson annihilation into a lower energetic state) is sometimes called the s-channel [4]. It is characterized by the unique (non-energy-conserving) intermediate (off mass shell) state $\|p + k\rangle\rangle$ and transition amplitude $\kappa_s \equiv \langle\langle p + k\|V\|p; k\rangle\rangle = \gamma c^{5/2}\Gamma(p,k)$. The upward transition (t-channel) excites the two-boson state $\|p - k_f; k, k_f\rangle\rangle$. The amplitude for this process is given $\kappa_t \equiv \langle\langle p - k_f; k, k_f\|V\|p; k\rangle\rangle = \gamma c^{5/2}\Gamma(p, -k_f)$. The other two couplings are $\kappa_{sf} \equiv \langle\langle p + k\|V\|p_f; k_f\rangle\rangle = \gamma c^{5/2}\Gamma(p + k, -k_f)$ and $\kappa_{tf} \equiv \langle\langle p - k_f; k, k_f\|V\|p_f; k_f\rangle\rangle = \gamma c^{5/2}\Gamma(p - k_f, k)$. To conserve the total energy, each of the intermediate states can couple back to the original state or to the state $\|p_f; k_f\rangle\rangle$.

In order to obtain an analytical estimate of the effective coupling strength from the state $\|p; k\rangle\rangle$ to the state $\|p_f; k_f\rangle\rangle$, we can adiabatically eliminate the two intermediate states $\|p + k\rangle\rangle$ and $\|p - k_f; k, k_f\rangle\rangle$. Inserting the state $\|\Phi(t)\rangle\rangle = \exp(-iEt)\{C(t)\|p; k\rangle\rangle + C_f(t)\|p_f; k_f\rangle\rangle + C_s(t)\|p + k\rangle\rangle + C_t(t)\|p - k_f; k, k_f\rangle\rangle\}$ into the Schrödinger-like equation $i\partial\|\Phi(t)\rangle\rangle/\partial t = H\|\Phi(t)\rangle\rangle$, we find four coupled differential equations for the amplitudes C, C_s, C_t, and C_f:

$$i\partial C/\partial t = \kappa_s C_s + k_t C_t, \quad (3.1a)$$

$$i\partial C_s/\partial t = \{E(p+k) - [E(p) + \omega(k)]\}C_s + k_s C + k_{sf}C_f, \quad (3.1b)$$

$$i\partial C_t/\partial t = [E(p-k_f) + \omega(k_f) - E(p)]C_t + k_t C + k_{tf}C_f, \quad (3.1c)$$

$$i\partial C_f/\partial t = \kappa_{sf}C_s + k_{tf}C_t. \quad (3.1d)$$

If we assume for the two off-resonant amplitudes $\partial C_s/\partial t \approx \partial C_t/\partial t \approx 0$, we can insert the expression from Eqs. (3.1b) and (3.1c) for $C_s(t) \approx -[\kappa_s C + \kappa_{sf}C_f]/[E(p+k) - E(p) - \omega(k)]$ and $C_t(t) \approx -[\kappa_t C + \kappa_{tf}C_f]/[E(p-k_f) + \omega(k_f) - E(p)]$ into the Eqs. (3.1a) and (3.1d), leading to an
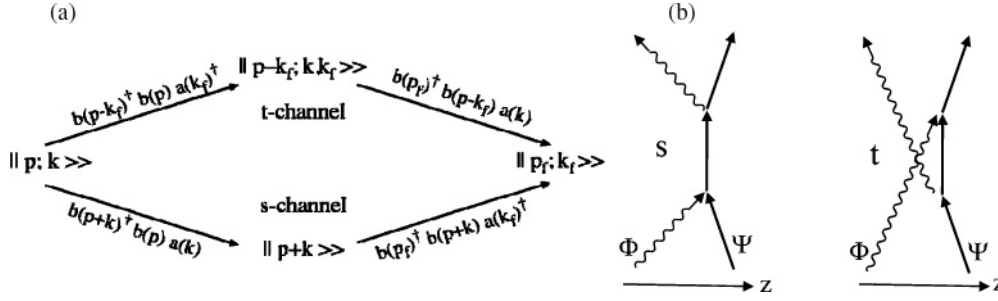
(a) (b)

FIG. 1. (a) The two lowest-order s- and t-scattering channels transferring the initial state $\| p; k \rangle\rangle$ to the final state $\| p_f; k_f \rangle\rangle$ of the same bare energy. (b) The corresponding Feynmann diagrams.

effective two-level system for $C(t)$ and $C_f(t)$ with the coupling

$$\langle\langle p_f; k_f \| H_{\text{eff}} \| p; k \rangle\rangle$$
$$= \gamma^2 c^5 \{ \Gamma(p + k, -k_f) \Gamma(p, k) / [E(p)$$
$$+ \omega(k) - E(p + k)] + \Gamma(p - k_f, k)$$
$$\times \Gamma(p, -k_f) / [E(p) - E(p - k_f) - \omega(k_f)] \}. \quad (3.2)$$

We have omitted the additional factor $\delta(0)$ associated with the conservation of the total momentum. The form of the coupling functions Γ was given after Eq. (2.3). It is important to note that the first term (associated with the s-channel) is positive, as $E(p) + \omega(k) > E(p+k)$, while the second term (t-channel) is negative, leading to destructive interferences with regard to the total amplitude as we will discuss in the following.

Without any loss of generality, from now on we view the dynamics with regard to the center-of-mass coordinate system such that we can set $k = -p$ and $p_f = -k_f = -p$. As a result the amplitude to connect the state $\| p; -p \rangle\rangle$ to $\| -p; p \rangle\rangle$ becomes a function of p only, and we define $V(p) \equiv \langle\langle -p; p \| H_{\text{eff}} \| p; -p \rangle\rangle$, which leads to

$$V(p) = \gamma^2 c^5 \Gamma(0, -p) \Gamma(p, -p) \{ 1 / [E(p) + \omega(k) - E(0)]$$
$$+ 1 / [E(p) - \omega(k) - E(0)] \}. \quad (3.3)$$

In Fig. 2 we graph $V_s(p)$ and $V_t(p)$ associated with the s- and t-channel only and show in the inset the resulting $V(p) = V_s(p) + V_t(p)$. We see that (except the signs) $V_s(p)$ and $V_t(p)$ are overall very similar. In fact, for small momentum, the amounts are identical, $V_s(0) = |V_t(0)| = \gamma^2 c / (4\pi m^2)$. For large values of the momentum p, however, their asymptotic behaviors are quite different: $V_s(p \to \infty) \to \gamma^2 c^3 / (16\pi) p^{-2}$ while $V_t(p \to \infty) \to -\gamma^2 c^2 / (8M\pi) p^{-1}$ and approaches zero from below at a much slower rate than V_s. This different asymptotic behavior is important when we introduce the Compton force field below.

To get a better qualitative understanding of the momentum dependence of the coupling, we can try to fit the coupling to a sum of two simple Lorentzians of the form: $V(p) \approx A_s / (p^2 + B_s) + A_t / (p^2 + B_t)$. If we equate the first- and second-order derivatives with respect to the momentum at $p = 0$, we find for the Lorentzian parameters $A_s = c^3 \gamma^2 r_+ / \pi$, $B_s = 4c^2 m^2 r_+$, $A_t = -c^3 \gamma^2 r_- / \pi$, and $B_t = 4c^2 m^2 r_-$. Here we have defined an effective mass ratio $r_\pm = 1 / [(m/M)^2 + 4 \pm 2(m/M)]$. As the ratio m/M increases, r_+ decreases from

$\frac{1}{4}$ to zero, while r_- rises first from $\frac{1}{4}$ to a maximum of $r_- = 1/3$ (for $m = M$) before it approaches zero. If we introduce the effective coupling strengths $V_{0s} \equiv \gamma^2 c^2 \mu^{1/2} m^{-3/2} / 2$ and $V_{0t} \equiv \gamma^2 c^2 \mu'^{1/2} m^{-3/2} / 2$, with the usual reduced bare mass of the system, $\mu \equiv mM/(M + m)$, and the semireduced mass, $\mu' \equiv mM/(M - m)$, we find for the Lorentzian approximations,

$$V_{\text{Lor}}(p) = V_{0s}(\mu m c^2)^{1/2} (2\pi)^{-1} [p^2 + \mu m c^2]^{-1}$$
$$+ V_{0t}(\mu' m c^2)^{1/2} (2\pi)^{-1} [p^2 + \mu' m c^2]^{-1}. \quad (3.4)$$

The dotted data in Fig. 2 show the excellent quality of the Lorentzian approximations $V_{s,\text{Lor}}(p)$ and $V_{t,\text{Lor}}(p)$, corresponding to the first and second terms in Eq. (3.4). For each channel separately, the corresponding graphs are nearly indistinguishable. However, the approximation $V_{\text{Lor}}(p)$ for the whole dynamics can only give a qualitative picture for the exact $V(p)$, as the differences between $V_s(p)$ and $|V_t(p)|$ are very small and unfortunately comparable to the error made by the Lorentzian approximation. We have compared the two graphs in the inset of Fig. 2.
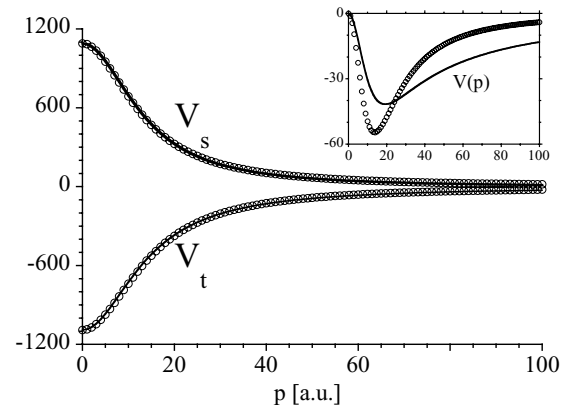

FIG. 2. The effective coupling strength $\langle\langle p_f; k_f \| H_{\text{eff}} \| p; k \rangle\rangle$ (graphed in units of γ^2) between the incoming state $\| p; -p \rangle\rangle$ and the scattered state $\| -p; p \rangle\rangle$ defined in Eq. (3.2) as a function of the momentum p for the s-channel (or t-channel) mechanism only. The dots show the approximate Lorentzian form given by Eq. (3.4). The net potential $V(p) = V_s(p) + V_t(p)$ is displayed in the inset with the corresponding Lorentzian fit $V_{\text{Lor}}(p)$ (dotted). (The parameters are fermion mass $M = 1$ a.u.; boson mass $m = 0.1$ a.u.)

B. The Compton force field

Next we will discuss how the quantum field theoretical system based on the absorption and re-emission of bosons can be modeled quantum mechanically by an effective spatially dependent potential $V_{qm}(z)$. The transition from a quantum field theory (where any elementary interaction is synonymous to a change in the number of particles) to the unitary theory of quantum mechanics (where interactions are approximated by forces) is nontrivial. It can be attempted if we simply equate the effective quantum field theoretical matrix element $V(p)$ [from Eq. (3.3)] with the corresponding matrix element between a left- and right-moving quantum mechanical state $\langle -p|V_{qm}|p\rangle = \langle\langle -p; p\|H_{\text{eff}}\|p; -p\rangle\rangle$. The full quantum mechanical two-particle matrix element would contain a factor $\delta(0)$ associated with the center-of-mass coordinates, which we have omitted here (similar to the corresponding omission with regard to $\langle\langle -p; p\|H_{\text{eff}}\|p; -p\rangle\rangle$). If we use the spatial representation of the Dirac quantum mechanical states $\langle z|p\rangle = (2\pi)^{-1/2}u(p)\exp(ipz)$, this would lead to the equation

$$\langle -p|V_{qm}|p\rangle = (2\pi)^{-1}\int dz \exp(i2pz)u(-p)^\dagger V_{qm}(z)u(p)$$
$$= V(p). \tag{3.5}$$

For simplicity let us assume that the effective quantum mechanical potential $V_{qm}(z)$ is proportional to the unit matrix. This approximation could possibly restrict the limit of validity of the potential to the nonrelativistic regime. To calculate the quantum mechanical potential, we use the simple inverse Fourier transformation, $V_{qm}(z) = \int dp \exp(-ipz)V(p/2)[u(-p/2)^\dagger u(p/2)]^{-1}$. This inversion has to be done numerically to compute the exact equivalent potential. In Fig. 3 we graph the numerically obtained potential for Compton scattering. The potential is singular at the origin. This singularity is related to the slow asymptotic behavior of $V_t(p) \sim 1/p$ for large momenta. However, this singularity could be a consequence of our assumption that the potential should be proportional to the unit matrix in spinor space, making the (relativistic) large-p limit unreliable. Furthermore, our analysis has included only the s- and t-channel states and higher-order coupled states could correct the large-p behavior
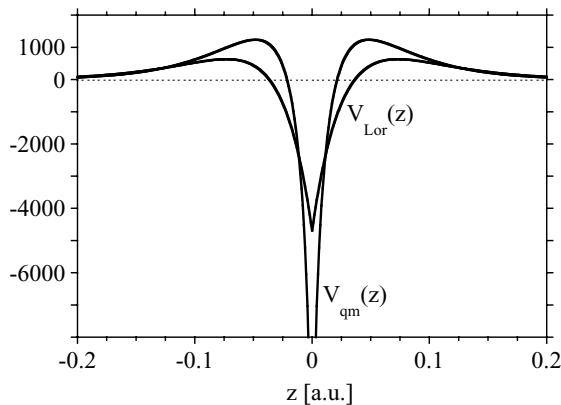

FIG. 3. The effective quantum mechanical potential $V_{qm}(z)/\gamma^2$ obtained from Eq. (3.5). The second curve $V_{\text{Lor}}(z)/\gamma^2$ is the approximation given by Eq. (3.6). (The parameters are fermion mass $M = 1$ a.u.; boson mass $m = 0.1$ a.u.)

of $\langle\langle -p; p\|H_{\text{eff}}\|p; -p\rangle\rangle$. The transition from the repulsive to the attractive area occurs at position $z = 0.048$, which is less than the reduced Compton wavelength of the boson, $1/(mc) = 0.073$. The energy of the repulsive barrier is about $633\gamma^2$; we will use this estimate in the following. The potential suggests that depending on the incoming momentum, there could be two different scattering mechanisms, one associated with either an effectively repulsive barrier and a corresponding large value for the minimum fermion-boson spacing (impact parameter) during the collision, and a closer contact collision for large momenta.

An analytical estimate for $V_{qm}(z)$ is possible again if we use the corresponding Lorentzian approximation $V_{\text{Lor}}(z)$. In this case we find the potential in coordinate space,

$$V_{\text{Lor}}(z) = V_{0s}\exp[-2m\kappa_+c|z|] + V_{0t}\exp[-2m\kappa_-c|z|]. \tag{3.6}$$

Here, we have introduced the dimensionless parameters $\kappa_\pm = 4M^2/(-m^2 + 4M^2 \pm 2mM)$ and $V_{0s} = c^3\gamma^2/(2mc\sqrt{\kappa_+})$ and $V_{0t} = -c^3\gamma^2/(2mc\sqrt{\kappa_-})$. Note that these coefficients are different from $r_\pm$ discussed previously. We see that the force associated with the s-channel is repulsive and has a slightly longer range (as $\kappa_+ < \kappa_-$), whereas the t-channel force is attractive and has a shorter effective range. For small momentum, the repulsive s-channel barrier therefore dominates the scattering while for large momentum [$p^2/(2\mu) > V_{0s}$] the attractive part of the force becomes important. In the interesting limit of vanishing boson mass, $m \to 0$, the approximate potential becomes attractive, $V_{qm}(z) = -c^2\gamma^2/(4M)\exp[-2mc|z|]$, where the range is determined solely by the boson mass while the strength scales inversely proportional to the fermion's mass M. The comparison with the exact potential shown in Fig. 3 shows a qualitative match, sufficient for analytical order of magnitude estimates.

IV. MONOCHROMATIC SCATTERING INSIDE A RING CAVITY

If we place the fermion and the boson into a ring cavity in which they are allowed to move with opposite momenta, the scattering can be studied from a different perspective. The interaction time can be chosen arbitrarily large and it is no longer limited by the duration of spatial overlap between the two wave packets. As a result of this new degree of freedom, we can study nonperturbative periodic and coherent processes that cannot be described by a differential cross section. For example, as the fermion and the boson interact (beginning from the initial state $\|p; -p\rangle\rangle$), the probability of the state $\|-p; p\rangle\rangle$ can become 100%, corresponding to a complete momentum reversal of each particle and 100% reflection. However, as this state evolves further in time, the state can evolve back to the initial state. In other words, we can have an almost periodic sequence of scattering events.

In Appendix A we show that the frequency Ω of these momentum reversals can be directly related to the coupling matrix element via $\Omega = (2\pi/L)|V(p)|$, where L denotes the total length of the ring cavity. This also allows us to relate the frequency to the reflection coefficient R via $\Omega = R^{1/2}p/(L\mu)$.
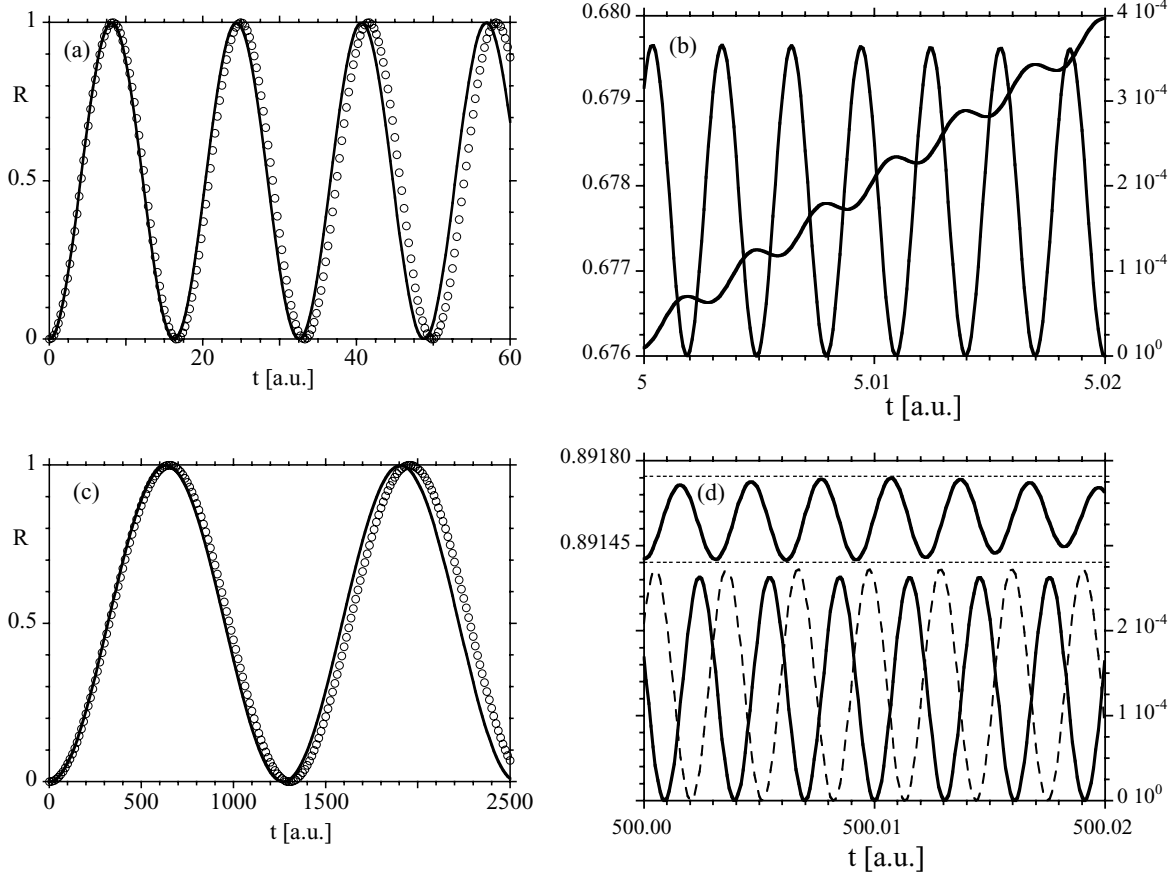
FIG. 4. (a) The time dependence of the probability of the state $|\langle\!\langle -p; p\|\Phi(t)\rangle\!\rangle|^2$ for the s-channel-only dynamics for $\gamma = 0.025$ and $L = 6\pi$. The initial state was $\|\Phi(t=0)\rangle\!\rangle = \|p; -p\rangle\!\rangle$. The dashed curve is $P(t) = \sin^2(\Omega t)$, where the Rabi frequency $\Omega = 1.89 \times 10^{-1}$ is obtained from $\Omega = (2\pi/L)\,|V_s(p)|$, where $V_s = 0.56667$. (b) The time dependence of the probability of the virtual intermediate state $\|p = 0\rangle\!\rangle$. The amplitudes are indicated by the right scale. For comparison, we also repeat the (rising) graph from Fig. 4(a) associated with the left scale. (c) The time dependence of the probability of the state $|\langle\!\langle -p; p\|\Phi(t)\rangle\!\rangle|^2$ for the complete dynamics (s- and t-channels) for $\gamma = 0.01$ and $L = 4\pi/3$. The dashed curve is $P(t) = \sin^2(\Omega t)$, where the Rabi frequency $\Omega = 2.41 \times 10^{-3}$ is obtained from $\Omega = (2\pi/L)\,|V_s(p) + V_t(p)|$, where $V_s = 9.06679 \times 10^{-2}$ and $V_t = -9.22734 \times 10^{-3}$. (d) The time dependence of the probability of the virtual intermediate states $\|p = 0\rangle\!\rangle$ and $\|p = 0; k = p, k = -p\rangle\!\rangle$. The top curve with left axis labels is $|\langle\!\langle -p, p\|\Phi(t)\rangle\!\rangle|^2$; bottom graphs are $|\langle\!\langle p = 0\|\Phi(t)\rangle\!\rangle|^2$ (continuous, s-channel) and $|\langle\!\langle p = 0; k = p, k = -p\|\Phi(t)\rangle\!\rangle|^2$ (dashed, t-channel with two-photon state). (The parameters were fermion mass $M = 1$ a.u., boson mass $m = 0.1$ a.u., and momentum $p = 6$.)

In Fig. 4(a) we have graphed the time evolution of the probability density $|\langle\!\langle -p; p\|\Phi(t)\rangle\!\rangle|^2$ for the s-channel only. The dots show the analytical estimate $P(t) = \sin^2 \Omega t$. The agreement is excellent and suggests that the two-level approximation which reduces the Hilbert space to only two states $\|p; -p\rangle\!\rangle$ and $\|-p; p\rangle\!\rangle$ and an effective coupling $V_s(p)$ is quite reasonable.

The good agreement between the graph and the analytical estimate suggests that the data are periodic; however, a zoomed-in view for a very small time interval [shown in Fig. 4(b)] reveals that the numerical data also contain additional high-frequency oscillations with very small amplitudes. These oscillations are a direct consequence of the back reaction of the virtual intermediate particles that are involved in the dynamics. The second graph in Fig. 4(b) shows the probability $P_{\rm virt}(t)$ of the intermediate state characteristic of the fermion at rest ($p = 0$) and no boson. This probability is defined as $P_{\rm virt}(t) = |\langle\!\langle p = 0\|\Phi(t)\rangle\!\rangle|^2$ and describes the virtual fermion at rest. We find that

this virtual particle probability is characterized by rapid oscillations.

We can get a rough estimate of the frequency and also the amplitude of the virtual particle dynamics. In the absence of any coupling ($\gamma = 0$), the energy difference between the initial and the intermediate state is given by $\Delta E_{\rm virt} = E(p) + \omega(k) - E(0)$, which can be associated with the time scale $2\pi/\Delta E_{\rm virt}$. As we have discussed in Sec. 2, the coupling strength between the initial state and the virtual state is given by $\kappa_s \equiv \langle\!\langle p = 0\|V\|p; -p\rangle\!\rangle = \gamma c^{5/2}\Gamma(p, -p)$. If we assume that the Hilbert space for the s-channel dynamics can be approximated by only two energy-degenerate levels with zero energy (corresponding to $\|p; -p\rangle\!\rangle$ and $\|-p; p\rangle\!\rangle$) and a lower-level (corresponding to the state $\|p = 0\rangle\!\rangle$) with energy $\Delta E_{\rm virt}$, then the effective three-level system can be solved analytically, predicting that $P_{\rm virt}(t) = |\langle\!\langle p = 0\|\psi(t)\rangle\!\rangle|^2 = (2\kappa_s/\Omega_{\rm virt})^2 \sin^2[\Omega_{\rm virt}t]$ with a characteristic frequency given by $\Omega_{\rm virt} \equiv \sqrt{(\Delta E_{\rm virt}^2 + 8\kappa_s^2/2)}$. For the parameters of the figure ($\kappa_s = 34.2$ and $\Delta E_{\rm virt} = 2068$), we find the period $\pi/\Omega_{\rm virt} \approx 2\pi/\Delta E_{\rm virt} = 0.003$,
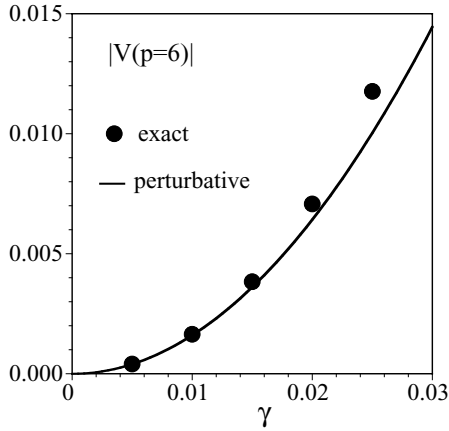
FIG. 5. The effective coupling strength $|V(p = 6)|$ as a function of the parameter γ. The continuous line is the prediction according to second-order perturbation theory leading to Eq. (3.1). (The parameters were fermion mass $M = 1$ a.u., boson mass $m = 0.1$ a.u., and momentum $p = 6$; ring-cavity length $L = 4\pi/3$.)

which fits perfectly with the data. However, the predicted amplitude $(2\kappa_s/\Omega_{\text{virt}})^2$ amounts to 4.3×10^{-3} and is much larger than the actual numerical amplitude of about 3.7×10^{-4}.

In the corresponding data in Figs. 4(c) and 4(d) we show the same quantities for the full dynamics by permitting any available state of the Hilbert space involving an arbitrary number of bosons. To ensure numerical convergence, the coupling was reduced to $\gamma = 0.01$ and the length of the resonator cavity was reduced to $L = 4\pi/3$. Once again, the agreement of $|\langle\langle p; -p\|\Phi(t)\rangle\rangle|^2$ with the approximate expression $\sin^2\Omega t$ is excellent. In order to determine the frequency $\Omega = (2\pi/L)\,|V(p)|$, both channels (with $V_s = 0.090\,667\,9$ and $V_t = -0.092\,273\,4$) had to be taken into account, leading to $\Omega = 2.4 \times 10^{-3}$. It is interesting to note that in contrast to the s-channel-only dynamics, the back reaction of the (at least) two intermediate states induces not only the rapid time scales associated with the energy offset of each virtual state, but also a more slow modulation which could be the result of a beating pattern associated with the different energies of the virtual states $\Delta E_s = 2068$ and $\Delta E_t = -2032$. To better visualize this effect, we have included into the upper graph in Fig. 4(d) two dashed parallel lines as a reference to show the slow variation of the amplitude $|\langle\langle p; -p\|\Phi(t)\rangle\rangle|^2$.

In order to observe some nonperturbative effects, we have increased the coupling strength and found that the motion remains quasiperiodic but the "frequency" is actually larger than predicted by the scaling $\Omega = (2\pi/L)\,|V(p)|$. This value was then used to compute the exact coupling strength $V(p)$ which is shown in Fig. 5 by the black dots. In the perturbative region the data obviously match, whereas for larger values we see some deviations. For example, for $\gamma = 2.5 \times 10^{-2}$ the exact coupling (1.17×10^{-2}) exceeds the perturbative value (10^{-2}) by 17%, while for $\gamma = 5 \times 10^{-3}$ the error is less than 1%.

V. COMPTON SCATTERING OF TWO WAVE PACKETS

Let us now discuss a one-time scattering event associated with two colliding spatially localized wave packets. We focus here on the dynamics associated with the s-channel only. To

model the localized fermion and boson, we use a Gaussian superposition of the (uncoupled) energy eigenstates $\|\Phi(t = 0)\rangle\rangle = \|\Phi_f\rangle\rangle\|\Phi_b\rangle\rangle$ where

$$\|\Phi_{f,b}\rangle\rangle = \int dp(2/\pi)^{1/4}\Delta_{f,b}^{1/2}\exp\left[-(p - p_{0f,b})^2\Delta_{f,b}^2\right]$$
$$\times \exp[ipz_{0f,b}]\|p\rangle\rangle. \tag{5.1}$$

The parameters z_0, p_0, and Δ are the initial location, the central momentum, and the spatial width of the state, respectively.

The space-time evolution of the state $\|\Phi(t)\rangle\rangle$ can be analyzed with respect to the properties of the underlying bare particles. The spatial distribution of the (bare) number density can be computed via $\rho_b(z,t) \equiv \langle\langle\Phi\|\hat{a}_z^\dagger\hat{a}_z\|\Phi\rangle\rangle$ and $\rho_f(z,t) \equiv \langle\langle\Phi|\hat{b}_z^\dagger\hat{b}_z|\Phi\rangle\rangle$, as discussed in standard textbooks [16]. Here $\hat{a}_z$ is the Fourier transform of the annihilation operator in momentum space, $\hat{a}_z \equiv (2\pi)^{-1/2}\int dk\hat{a}_k\exp(ikz)$, and correspondingly for $\hat{b}_z$. When integrated over the whole space, we obtain the total number of bosons, $N_b = \int dz\langle\langle\hat{a}_z^\dagger\hat{a}_z\rangle\rangle$, such that the ratio $\langle\langle\hat{a}_z^\dagger\hat{a}_z\rangle\rangle/N_b$ can be interpreted as the spatial probability density. Due to the conservation law of the fermion number, we always have $\int dz\langle\langle\hat{b}_z^\dagger\hat{b}_z\rangle\rangle = 1$.

In Fig. 6 we give an example of a scattering event. Figure 6(a) shows the spatial distributions $\rho_f(z,t)$ and $\rho_b(z,t)$ before and after the scattering of the fermion and boson. While the low-mass boson ($m = 0.1$) has an (almost relativistic) velocity of $v = c^2 p/\omega(p) = 54.96$ and can travel from $z_{0b} = -5$ to $z(t) = 12.58$ during $t = 0.32$, the heavier fermion (with speed $v = -6$) can only pass from $z_{0f} = 3.5$ to $z(t) = 1.58$. From the graphs we see the center of the reflected (transmitted) boson wave packet at $z = 12.56$ ($z = -7.1$), whereas the reflected fermion did not have sufficient time to fully separate from the transmitted portion.

Figure 6(b) shows that the corresponding snapshots with momentum resolution give a much more detailed picture of the process and allow us to observe the reflected wave packet portions of both particles as well as the virtual particles associated with the intermediate s-channel state. It is interesting to note that at intermediate times (such as $t = 0.14$) the maximum momenta associated with the scattered portions are at a momentum larger than p. For the fermion the probability peaks at $p = -6.1$, while the boson is shifted to $p = 6.1$. This could be related to the fact that the larger momentum components of the states collide earlier in time than the slower portions associated with the central peaks. At the final time the peak centers are closer to $p = \pm 6$. As the scattering strength depends quite sensitively on the relative momentum, it is not guaranteed that the scattered wave packets are still Gaussian and that the largest scattering occurs at the momentum with the largest amplitude, $p = 6$.

It is interesting to also observe the momentum distribution close to $p = 0$ associated with the intermediate state. Its weight starts at zero and it reaches its largest value around $t = 0.14$ when the fermion and boson have their largest overlap. Once the scattering is completed the weight of these virtual zero-momentum fermions decreases back to zero.

Let us now analyze how the reflected portion of the fermion (and equivalently of the boson) changes as a function of time.
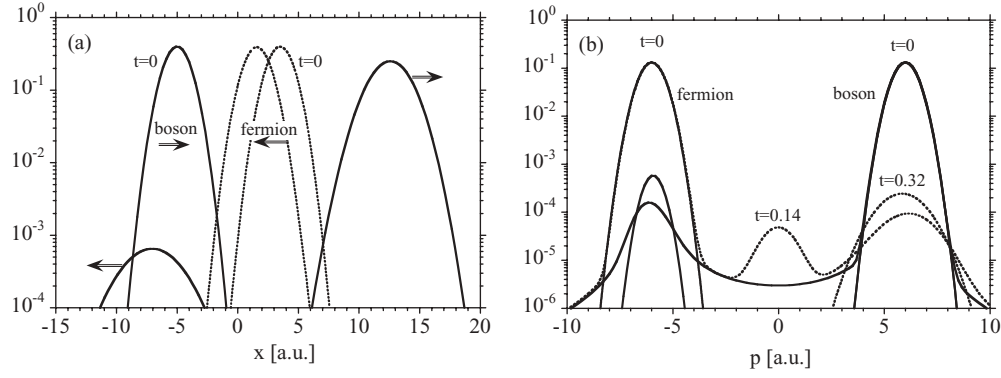
FIG. 6. (a) Spatial snapshots of the scattering of fermion $\rho_f(z,t)$ (dashed line) and boson wave packets $\rho_b(z,t)$ at time $t = 0$ and 0.32. (b) The same dynamics but graphed in the momentum space $\rho_f(p,t)$ and $\rho_b(p,t)$ for time $t = 0, 0.14, 0.32$. [The parameters were fermion mass $M = 1$ a.u., boson mass $m = 0.1$ a.u.; the initial location, spatial width, and momentum of the fermion (boson) are $z_{0f} = 3.5$ ($z_{0b} = -5$), $\Delta z_f = 1(\Delta x_b = 1)$, and $p = -6$ ($k = 6$); the numerical box $L = 12\pi$ was discretized into 141 grid points, $\gamma = 0.025$, and the maximum available photon number was restricted to 1 to focus on the effects of the s-channel dynamics only.]

In Fig. 7 we analyze the scattering event with regard to the time-dependent portions. The reflected portion of the fermion can be obtained from either the spatial density $\int_{-\infty}^{-0.75} \rho_f(z,t)\,dz$ [where $(z_{0f} + z_{0b})/2 = -0.75$ is the center of mass], or from the integral over the momentum density, $\int_2^\infty \rho_f(p,t)dp$. It turns out that while these two expressions become identical in the long time limit when the reflected and transmitted portions no longer overlap, the definition based on the momentum approaches this limit in shorter time. We therefore graph $\int_{-\infty}^{-2} \rho_f(p,t)dp$, $\int_{-2}^{2} \rho_f(p,t)dp$ and $\int_2^\infty \rho_f(p,t)dp$ in Fig. 7. In Appendix B we suggest that in the nonrelativistic regime the momentum dependence of the reflection coefficient can be calculated from the effective matrix element $R_{pert}(p) = (2\pi \mu V(p)/p)^2$. For the parameters in our numerical example ($p = 6$) and the s-channel this predicts a reflected amount of $R_{pert} = 2.91 \times 10^{-3}$ (for the s-channel with $V_s = 0.56667$). The true amount of the reflected portion of the fermion is about 3.6×10^{-3}; this means that the prediction differs by 24%. This discrepancy could be related to several mechanisms.
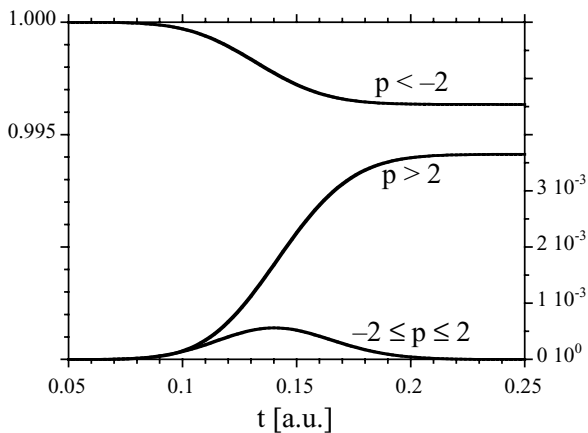

FIG. 7. The time dependence of the probability for the transmitted portion ($p < -2$) according to the left scale. The much less likely virtual particles ($-2 < p < 2$) and the reflected portion ($2 < p$) are shown by the right axis. (Same parameters as in Fig. 6 but $p = -6$.)

First, the graph in Fig. 7 represents the reflection of all momentum components. For a fairer comparison we have computed a momentum averaged reflection, $\int_{-\infty}^{\infty} \rho_f(p,t = 0)$ $R_{pert}(p)dp$ which amounted to almost the same value $\langle R_{pert}\rangle = 2.91 \times 10^{-3}$, so the discrepancy is not related to the quantum mechanical momentum uncertainty (here $\Delta p = 0.5$) in the wave packet.

The second possible source for a discrepancy is related to the perturbative nature of the expression $R_{pert}(p) = (2\pi \mu V(p)/p)^2$, which is only valid under the constraints discussed in Appendix B. To study its validity, we have performed a quantum mechanical wave packet simulation representing an effective particle with the reduced mass μ scattering off the (approximate analytical) potential $V_{qm}(z)$ described by Eq. (3.5). We found $R_{qm} = 2.73 \times 10^{-3}$, which is significantly closer to the predicted value, suggesting that the perturbative nature of the expression for R_{pert} is also not likely to be the source for the 24% discrepancy found here.

We believe the main source of the discrepancy might be the fact that the numerical dynamics also contain significant couplings between other quantum field theoretical momentum states than $p = -6$ (fermion) and $p = 6$ (boson) that have been excluded in our simplified numerical analysis as the derivation in the appendix assumed two fully monoenergetic wave packets, corresponding to the limit $\Delta p \to 0$. This approximation does not take the dynamics of other momenta into account which are unavoidably also part of the wave packet. In fact, the fully monoenergetic limit discussed in Sec. IV agreed almost perfectly with the expression $R_{pert} = (2\pi \mu V(p)/p)^2$.

As the scattering of a boson with a fermion requires intermediate states (virtual particles associated with the s- and t-channels) it does not occur instantaneously. In other words, the boson emission and absorption processes happen on nonzero time scales that could have an impact on the spatial structure of the final state of the scattered fermion and boson. In the monoenergetic scattering setup [shown in Figs. 4(b) and 4(d)] we showed that the (periodic) lifetime of the virtual states defined as the period of the oscillations was given by $2\pi/\Delta E_{virt}$, which amounted to about $\Delta T_{virt} = 3 \times 10^{-3}$

(*s*-channel) and 3.1×10^{-3} (*t*-channel) for our parameters ($M = 1$, $m = 0.1$). In the opposite limit of wave-packet scattering (shown in Fig. 7), the lifetime of the virtual states is much longer and directly proportional to the overlap time ΔT of the wave packets given by the ratio of the spatial widths and the relative velocities of the particles. The energy width of the particles averages out the fine monochromatic oscillations on the smallest energy scale ($2\pi/\Delta E_{\text{virt}}$), leading to the lifetime of about $\Delta T_{\text{coll}} = 0.1$ (Fig. 7). In the center-of-mass frame, the two lowest-order intermediate states describe a (virtual) fermion with vanishing momentum, which could lead to a characteristic time delay of the scattering process. In other words, this delay could lead to a similar spatial offset as observed in the Goos-Hänchen effect associated with tunneling in frustrated total reflection [19,20]. For our parameters [velocity $v = c^2 p/\omega(p) = 54.96$], a delay of 3×10^{-3} would lead to a spatial offset $\Delta z_b = v\Delta T_{\text{virt}} = 0.16$. The center from Fig. 6(a) is about $z_f(t) = 12.56$, which is very close to $z_f(t) = z_{0f} + vt = 12.58$, so the offset cannot be seen in the data. In Appendix B we have shown that the transmitted fermion is a superposition of the (unattenuated) incoming and the forward scattered portion [with amplitude $d\sigma(+) = (|f+\rangle)|^2$] of the fermion. As only the (very small) forward scattered portion should be affected by the delay, it is very difficult to confirm or disprove the predicted spatial shift from our data. As the final time is too short with regard to the slowly moving (more massive) fermion to fully separate the reflected and transmitted wave packets, it is difficult to observe a delay in the reflected portion. While the momentum resolved data in Fig. 6(b) allow a unique identification of the reflected fermion, they do not contain sufficient information about the spatial properties.

VI. DISCUSSION AND QUESTIONS

In this work we have suggested that the Compton scattering of a fermion with an incoming boson can be modeled quantum mechanically in the center-of-mass frame by a partially repulsive and partially attractive force field, described by the potential $V_{qm}(z)$. This potential was obtained by equating the quantum field theoretical matrix element with an effective interaction obtained by adiabatically eliminating the intermediate *s*- and *t*-channel virtual states with the corresponding quantum mechanical transition matrix element. For a sufficiently deep potential, it could have bound states. It might be very interesting to examine the dynamical significance of these Compton bound states on the original scattering dynamics. It could very well be that these bound states occur only for very large potential depth V_0, for which the perturbative approach becomes invalid.

As the coupling strength is increased, a wide variety of new phenomena can now be studied concerning boson splitting, the boson dressing of the fermion, and the impact of the coupling to positrons. For example, the state consisting of a fermion and an incoming boson could also evolve into a state in which the fermion is accompanied by two bosons at roughly half the frequency. This boson splitting process has the same momentum and energy as the initial state but its probability amplitude is proportional to γ^4.

In our simulation we have started the time evolution with the direct product of the bare fermion and boson state. It turns out that the fermion by itself is not stable and would emit bosons even without having scattered with the incoming boson [12]. It might be quite interesting to examine the effect of the boson dressing associated with a physical (and not bare) fermion on the scattering process. Again, as the scattering is of $O(\gamma^2)$, these corrections would scale with $O(\gamma^4)$.

While the fermionic field operator also contains the antifermion, the corresponding coupling was neglected in the Hamiltonian. The full formalism, however, becomes more complicated as the Hamiltonian requires renormalization. In this case, we would expect that the scattering between the fermion and the boson should also be accompanied by virtual antifermions. Our preliminary results indicate that the impact of antifermions is negligible for small coupling strength.

The final and most important question concerns the applicability of the concept of a Compton force to a boson of mass 0 and spin 1. While the massive bosons of spin 0 modeled by the Yukawa Hamiltonian are much easier to be treated theoretically, the ultimate goal would be to use the exact QED Hamiltonian to study the full three-dimensional time evolution of a photon interacting with an electron.

APPENDIX A

Here we will briefly show how, for the quantum mechanical situation described in Appendix B, the scattering coefficients need to be modified, if the scattering happens repeatedly between two perfectly monochromatic waves that have been placed in a ring cavity of total length L with $L/2 > a$. This system can be modeled if we assume that the wave function has to fulfill the boundary condition $\psi(z = -L/2, t) = \psi(z = L/2, t)$. As a result, we could restrict $-L/2 < z < L/2$ and normalize the states based on the Kronecker symbol as $\langle P'|P\rangle = \delta_{P,P'}$. With this convention we would obtain $\langle -P|V|P\rangle = -V_0 \sin(2Pa)/(LP)(\equiv W_1)$ and similarly $\langle P|V|P\rangle = -V_0 a/(2L)(\equiv W_2)$. Due to energy conservation, only the states $|P\rangle$ and $|-P\rangle$ are coupled. The effective two-level Hamiltonian between the right- and left-going states (denoted by $|+\rangle$ and $|-\rangle$) reads $H = [p^2/(2\mu) - W_2]|-\rangle\langle-| + [p^2/(2\mu) - W_2]|+\rangle\langle+| + W_1(|+\rangle\langle-| + |+\rangle\langle-|)$. If we diagonalize this Hamiltonian to find the energy eigenstates and eigenvalues, we can construct the time evolution of the initial state $|\psi(t = 0)\rangle = |+\rangle$. The projection onto the left-going state gives us $|\langle-|\psi(t)\rangle|^2 = \sin^2(\Omega t)$, where the effective Rabi frequency is given by $\Omega = |V_0 \sin(2Pa)/(LP)|$. If we relate this frequency to the matrix element for the scattering situation in Appendix B, we find the general final result,

$$\Omega = (2\pi/L)|V_{-p,p}|. \tag{A1}$$

This also allows us to relate the reflection coefficient that characterizes a (one-time) scattering event to the Rabi frequency for the ring-cavity system of length L (permitting

repeated scatterings) via $\Omega = R^{1/2} p/(L\mu)$. This shows the quite intuitive result that the scattering frequency Ω is just the product of the square root of the reflection coefficient (the backward scattering amplitude $|f(-)|$) divided by the time ($= L\mu/p$) it takes the particle of momentum p to pass the required distance L to return to the scattering site.

APPENDIX B

Here is a quick review showing that the same quantum mechanical partial wave formalism based on phase shifts can be applied to one-dimensional scattering [21,22]. In this formulation we have

$$\phi(z) = \exp(ipz) + f(\varepsilon)\exp(ip|z|), \qquad \text{(B1)}$$

where $\varepsilon = \pm$ and $f(\pm)$ is the scattering amplitude in the forward and backward directions. These amplitudes lead to the differential cross sections $d\sigma(-) = |f(-)|^2$ and $d\sigma(+) = |f(+)|^2$, and the total cross section is $\sigma_{\text{tot}} = |f(-)|^2 + |f(+)|^2$. As a consequence of the conservation of the norm, we have $|f(\pm)|^2 < 1$ such that the total cross section is confined to $0 < \sigma_{\text{tot}} < 4$.

Alternatively, the scattering can also be described by the reflection and transmission coefficients R and T. These can be found from the complex scattering amplitudes via $R = |f(-)|^2$ and $T = |1 + f(+)|^2$. While the sum of these coefficients always adds up to one, $R + T = 1$, the amplitudes for the forward and backward scattering are independent of each other and determine the angular distribution only if the wave has scattered. The scattering probability is described by the total cross section and cannot be found simply from R or T. As a result, we note that the set $\{d\sigma(-), d\sigma(+)\}$ is not uniquely related to the set $\{R, T\}$.

It is interesting to note that in this framework the extreme asymmetric case of zero transmission ($T = 0$) is possible only due to a very strong forward scattered wave $\exp(ipz)$

with amplitude $f(+) = -1$ that leads to a perfect destructive cancellation with the incoming wave $\exp(ipz)$. This situation is associated with equal differential cross sections for both directions, $d\sigma(-) = d\sigma(+)$. The opposite limit of a perfect transmission ($T = 1$) occurs if the amplitude fulfills $f(+) = \exp(i\phi) - 1$, which for $\phi = 0$ contains the interesting case of the complete absence of any forward scattered wave, $f(+) = 0$. While the phase of the amplitude for the backward scattered wave $f(+)$ has no impact on either the reflection coefficient or the differential cross section, the transmission coefficient depends sensitively on the phase of the forward scattered wave.

The main question for us is how the coefficients are related in the perturbative regime. For example, the scattering of a mass μ with an attractive square-well potential $V(z) = -V_0 \theta(z + a)\theta(-z + a)$ has the exact scattering amplitudes $f(-) = [\exp(2i\delta_0) - \exp(2i\delta_1)]/2$ and $f(+) = [i\exp(i\delta_0)\sin(\delta_0) + i\exp(i\delta_1)\sin(\delta_1)]$, where the exact phase shifts are given by $\delta_0 = \tan^{-1}\{\beta/p\tan(\beta a)\} - pa$ and $\delta_1 = \tan^{-1}\{p/\beta\tan(\beta a)\} - pa$ with $\beta = \text{sqrt}(p^2 + 2\mu V_0)$. The corresponding perturbative matrix elements are $V_{-p,p} \equiv \langle -p|V|p\rangle = -V_0\sin(2pa)/(2\pi p)$ and similarly $V_{p,p} \equiv \langle p|V|p\rangle = -V_0 a/\pi$, where the states are normalized on a momentum scale, $\langle p'|p\rangle = \delta(p' - p)$. Let us assume that $V_0 \ll p^2/(2\mu)$. The exact scattering amplitudes can then be expanded in V_0, leading to $f(-) = i\mu V_0 \sin(2pa)/p^2 - (\mu V_0)^2 \sin(2pa)/p^3$ and $f(+) = i\mu V_0 2ap - (\mu V_0)^2[(2ap)^2 + \sin^2(2pa)]/(2p^4)$. If we express the leading terms in terms of the matrix elements we obtain the results $f(-) = -2\pi i\mu V_{-p,p}/p$ and similarly $f(+) = -2\pi i\mu V_{p,p}/p$. We will use the corresponding expression for the perturbative reflection coefficient $R = (2\pi\mu V_{-p,p}/p)^2$ in the main text. We note that the reflection coefficient only depends on the matrix element and the incoming velocity($=p/\mu$), but not on the mass μ.

[1] A. H. Compton, Phys. Rev. **21**, 483 (1923); **22**, 409 (1923).
[2] S. S. Schweber, *An Introduction to Relativistic Quantum Field Theory* (Harper & Row, New York, 1962).
[3] C. Itzykson and J. Zuber, *Quantum Field Theory* (McGraw-Hill, New York, 1980).
[4] M. E. Peskin and D. V. Schroeder, *An Introduction to Quantum Field Theory* (Westview, Boulder, 1995).
[5] Frank Wissmann, *Compton Scattering, Investigating the Structure of the Nucleon with Real Photons* (Springer, Berlin, 2004).
[6] E. V. Stefanovich, Ann. Phys. (NY) **292**, 139 (2001).
[7] E. V. Stefanovich, e-print arXiv:hep-th/0503076v4.
[8] E. V. Stefanovich, e-print arXiv:physics/0504062v10 [physics.gen-ph].
[9] T. Cheng, E. R. Gospodarczyk, Q. Su, and R. Grobe, Ann. Phys. (NY) **325**, 265 (2010).
[10] O. W. Greenberg and S. S. Schweber, Nuovo Cimento **8**, 378 (1958).
[11] R. Walter, Nuovo Cimento A **68**, 426 (1970).
[12] T. Cheng, Q. Su, and R. Grobe, Opt. Commun. **283**, 1008 (2010).

[13] T. Cheng, C. C. Gerry, Q. Su, and R. Grobe, Europhys. Lett. **88**, 54001 (2009).
[14] R. E. Wagner, M. R. Ware, Q. Su, and R. Grobe, Phys. Rev. A **81**, 052104 (2010).
[15] L. Allen and J. H. Eberly, *Optical Resonance and Two-Level Atoms* (Dover, New York, 1975).
[16] L. Mandel and E. Wolf, *Optical Coherence and Quantum Optics* (Cambridge University Press, New York, 1995).
[17] C. C. Gerry and P. L. Knight, *Introductory Quantum Optics* (Cambridge University Press, Oxford, 2004).
[18] I. P. Grant and J. Sapirstein, in *Atomic Molecular & Optical Physics Handbook*, edited by G. W. F. Drake (AIP, Woodbury, 1996).
[19] W. Harshawardhan, Q. Su, and R. Grobe, Phys. Rev. E **62**, 8705 (2000).
[20] F. Goos and H. Hänchen, Ann. Phys. **436**, 333 (1947).
[21] J. H. Eberly, Am. J. Phys. **33**, 771 (1965).
[22] V. E. Barlette, M. M. Leite, and S. K. Adhikari, Eur. J. Phys. **21**, 435 (2000).